JOURNAL OF SOLID STATE CHEMISTRY 73, 452–467 (1988)

Study of the Crystal Structures of ZrSb and β-$ZrSb_2$ and of the Bonding in the Two $ZrSb_2$ Structures

EDUARDO GARCIA AND JOHN D. CORBETT

Ames Laboratory and Department of Chemistry, Iowa State University, Ames, Iowa 50011*

Received April 20, 1987; in revised form September 11, 1987

The structures of ZrSb and β-$ZrSb_2$ have proven to be orthorhombic with, respectively, a = 3.827(1), 7.393(1) Å, b = 10.426(3), 3.9780(7) Å, c = 14.007(5), 9.581(1) Å; space group *Cmcm*, *Pmma*; Z = 12, 4; R = 0.037, 0.032; R_w = 0.045, 0.039, for 327 and 345 independent reflections with $2\theta \leq 55°$. The new ZrSb structure can be described in terms of sheets of interlinked cofacial trigonal prismatic chains of zirconium centered by antimony that are separated by layers of weakly bonded antimony resembling those in the element. The substoichiometric β-form of $ZrSb_2$ ($ZrSb_{1.96}$) has a $PbCl_2$-type structure and contains zigzag chains of antimony atoms [d(Sb–Sb) = 2.89 Å] more weakly bonded to other antimony atoms to form ribbons. Some of the same features occur in the previously known α-$ZrSb_2$ modification. The electronic interactions of the two $ZrSb_2$ structures are compared with the aid of extended-Hückel density-of-states calculations. The heteroatomic bonding is dominant, with stronger Sb–Sb bonding in α-$ZrSb_2$. Significant Zr–Sb covalence, interantimony bonding, and the broad Zr–Sb valence band that results in β-$ZrSb_2$ remove it from the class of simple Zintl phases. Both compounds are predicted to be metallic, and α-$ZrSb_2$ is confirmed to exhibit metallic behavior ($\rho_{298} \sim 1.2 \times 10^{-4}$ ohm cm).

Introduction

A recent, thorough synthetic study of the binary zirconium–antimony system revealed that a total of 10 phases were formed (*1*). Good single crystals of two of these, ZrSb and $ZrSb_2$, were obtained by vapor phase transport with ZrI_4 and CdI_2, respectively. Their structural determinations are reported herein. The first occurs in a new structure type and the second in the broad class of $PbCl_2$ types. Structural differences between the new (β) $ZrSb_2$ structure and that of the previously reported (α) $ZrSb_2$ ($TiAs_2$-type) (*2*) have prompted a comparison of their bonding via extended-Hückel band calculations. This appears to be especially worthwhile as these phases are near the boundary where classical valence (e.g., 8-N) rules can be successfully applied.

Experimental Methods

Single-crystal X-ray studies. The synthetic routes are described elsewhere, as are the powder diffraction experiments (*1*). Single-crystal investigations of samples sealed in glass capillaries were carried out with the aid of a four-circle Ames Labora-

* The Ames Laboratory is operated for the U.S. Department of Energy by Iowa State University under Contract No. W-7405-Eng-82. This research was supported by the Office of Basic Energy Sciences, Materials Sciences Division.

0022-4596/88 $3.00

tory diffractometer equipped with a monochromator and using MoKα radiation. Programs for data averaging, absorption correction, Fourier synthesis, and least-squares refinement and the sources of scattering factors (including anomalous dispersion corrections) have been previously referenced (*3*). Tables of structure factors and thermal parameters are available, upon request, from one of the authors (J.D.C.).

ZrSb. Oscillation and Weissenberg photographs of a rectangular plate showed that ZrSb crystallizes with *C*-centered orthorhombic symmetry. The approximate lattice parameters so obtained allowed the powder pattern to be indexed and provided the refined values listed in Table I. Since the structure type of this compound could not be determined from the powder data, a single-crystal structural determination was carried out.

TABLE I

CRYSTAL AND DIFFRACTION DATA DETAILS FOR ZrSb AND $ZrSb_{1.96}$

Compound	ZrSb[a]	$ZrSb_{1.96}$
Lattice parameters (Å)[b]		
a (Å)	3.827(1)	7.393(1)
b (Å)	10.426(3)	3.9870(7)
c (Å)	14.007(5)	9.581(1)
V (Å^3)	558.9(3)	282.42(7)
Space group	*Cmcm*	*Pnma*
Z	12	4
d_{calc} (g/cm^3)	7.62	7.76
Crystal shape	Rectangular plate 0.27 × 0.18 × 0.05 mm	Rod 0.30 × 0.08 × 0.05 mm
Radiation	Graphite-monochromated MoKα	Graphite-monochromated MoKα
μ (cm^{-1})	196	223
Scan method (t°C)	$\omega - 2\theta$, 22°	$\omega - 2\theta$, 22°
Data collected	$\pm h, k, l$; $0° \leq 2\theta \leq 55°$	$\pm h, k, l$; $0° \leq 2\theta \leq 55°$
No. of data checked	762	775
No. of data $F_o^2 > 3\sigma(F_o^2)$	644	664
No. of unique data	327	345
R (av)	0.015	0.039
No. of variables	22	22
R on F_o	0.037	0.032
R_w on F_o	0.045	0.039

[a] Crystal from reaction [*10*], Ref. (*1*).
[b] From Guinier data.

Experimental details of data collection are given in Table I. The averaged data exhibited systematic absences consistent with the space group *Cmcm*. Initial determination of the positional parameters for two antimony atoms was accomplished by the use of MULTAN 80 (*4*), and a Fourier F-map following refinement of these positions revealed the location of the two zirconium atoms. Full-matrix, least-squares refinement with anisotropic thermal parameters proceeded smoothly. In the latter stages of the refinement, the multiplicities of three of the four atoms were allowed to vary with the result that all positions were found to be fully occupied (refined formula $ZrSb_{0.96(1)}$). The final refinement cycle converged at $R = 0.037$ and $R_w = 0.058$. Because weaker reflections were observed to have larger values of $w\Delta^2$ ($\Delta = |F_o| - |F_c|$, $w = \sigma_F^{-2}$), the data set was reweighted in six overlapping groups sorted according to F_o so that $w\Delta^2$ values for all the groups were equal. The final agreement factors were $R = 0.037$ and $R_w = 0.045$. A final electron density difference map revealed no residual greater than 1 e/Å^3.

β-ZrSb$_2$. A single crystal allowed the unit cell dimensions to be approximated by oscillation and Weissenberg techniques, and the precise lattice parameters given in Table I were then obtained by a least-squares fit to indexed Guinier powder diffraction data. The cell was found to be primitive orthorhombic. The small unit cell and especially the short b-axis indicated that this was most likely a previously unreported Zr–Sb binary compound, and a structural determination was deemed appropriate.

The diffraction data exhibited multiplicities and systematic extinctions consistent with the space group *Pnma*. Because of the synthetic route used (*1*), the composition of the sample was not known, but MULTAN 80 (*4*) rendered atomic positions and relative electron densities from which it became evident that the structure was com-

posed of three independent atoms, each with a fourfold multiplicity, and that the stoichiometry was $ZrSb_2$. A shift of the origin revealed that the structure was actually the anti-Co_2Si (*5*) or $PbCl_2$ type which is also known for ZrP_2 (*6*) and $ZrAs_2$ (*7*).

Full-matrix, least-squares refinement proceeded smoothly, and in the final cycle all positional, thermal, and occupancy parameters except the Zr multiplicity were allowed to vary. This revealed a slight deficiency of Sb(1) and an overall composition of $ZrSb_{1.956(4)}$. Since there was attack of the glass during the synthesis of this compound (*1*), the possibility that it was interstitially stabilized by either silicon or oxygen was considered, but a final electron density difference map did not contain any residual peaks greater than 0.5 $e/Å^3$.

Calculations

Three-dimensional, extended-Hückel band calculations were carried out on the two $ZrSb_2$ structural modifications using the atom positional parameters derived from single-crystal structural investigations.

The program utilized was developed and modified by Hoffmann and co-workers (*8*). The parameters utilized are listed in Table II. The H_{ii} values for zirconium 4*d*, 5*s*, and 5*p* orbitals were obtained by a linear interpolation between the parameters for Mo (*9*) and Y (*10*), whereas the antimony 5*s* and 5*p* values were included in the program package. The exponents and coefficients of the double-ζ expansion for zirconium 4*d* orbitals and single-ζ expansion for all other orbitals used to calculate the radial distribution function were as tabulated (*11*). All overlap integrals were evaluated to a distance of 9.1 Å beyond which they were set equal to zero. The density-of-states (DOS) curves were calculated by using 125 and 27 evenly spaced, symmetry-weighted *k* points in the three-dimensional Brillioun zone for the $PbCl_2$-type and $ZrSb_2$ structures, respectively, and were smoothed with a Gaussian function of 0.1 eV half-width at half maximum.

TABLE II

EXTENDED-HÜCKEL INPUT PARAMETERS

Atoms	Orbital	H_{ii} (eV)	ξ_1	ξ_2	C_1	C_2
Zr	4*d*	−8.12	3.84	1.505	0.6213	0.5798
	5*s*	−8.19	1.82			
	5*p*	−4.63	1.78			
Sb	5*s*	−18.80	2.32			
	5*p*	−11.68	2.00			

The nonstoichiometry of $ZrSb_{1.96}$ cannot be explicitly addressed by these calculations, but a rigid band approximation was applied in which the DOS curve calculated on the basis of $ZrSb_2$ was filled with 55 valence electrons to give a $(ZrSb_{1.95})_4$ unit cell composition.

Resistivity of $ZrSb_2$

Resistivity measurements were made on a single crystal of $ZrSb_2$ (α-structure) 4.0 × 0.2 × 0.2 mm in size that had been grown by a flux method (*1*). A standard four-probe, low frequency (22 Hz) AC technique was employed along the long dimension of the crystal (*c*-axis). The data were collected as the sample was being cooled.

Results

Crystal Structures

ZrSb. This orthorhombic phase represents a new structure type. The refined positional and thermal parameters and important interatomic distances are listed in Table III.

The principal bonding in ZrSb appears to be heteroatomic although layers of antimony(2) are also present. The Zr–Sb distances range from 2.84–3.11 Å (Table III) and as such probably represent strong bonding interactions when compared with 2.9–3.1 Å in the two forms of Zr_5Sb_3 (*12*)

TABLE III

REFINED PARAMETERS FOR AND DISTANCES IN ZrSb

Atom	Site	x	y	z
Zr(1)	8(f)	0	0.0714(1)	0.1088(1)
Zr(2)	4(c)	0	0.3798(2)	$\frac{1}{4}$
Sb(1)	4(c)	0	0.6694(1)	$\frac{1}{4}$
Sb(2)	8(f)	0	0.6415(1)	0.5477(1)

Interatomic distances (Å)[a]

Sb(1)–2Zr(2)	2.913(2)	Zr(1)–2Sb(1)	2.934(1)
Sb(1)–4Zr(1)	2.934(1)	Zr(1)–2Sb(2)	2.998(1)
Sb(1)–1Zr(2)	3.019(2)	Zr(1)–2Sb(2)	3.054(1)
		Zr(1)–1Sb(2)	3.113(2)
Sb(2)–1Zr(2)	2.835(1)	Zr(1)–1Zr(1)	3.385(2)
Sb(2)–2Zr(1)	2.998(1)	Zr(1)–2Zr(2)	3.399(1)
Sb(2)–2Zr(1)	3.054(1)		
Sb(2)–1Zr(1)	3.113(2)	Zr(2)–2Sb(2)	2.835(1)
Sb(2)–1Sb(2)	3.238(2)	Zr(2)–2Sb(1)	2.913(2)
Sb(2)–2Sb(2)	3.251(1)	Zr(2)–1Sb(1)	3.019(2)
		Zr(2)–4Zr(1)	3.399(1)

[a] Distances <3.5 Å.

and in $ZrSb_2$ (*2*). On the other hand, the Zr–Zr distances at 3.40 Å are fairly long, and only weak direct interactions between the transition metal atoms are expected. The Sb(2)–Sb(2) separations of 3.25 Å are intermediate in distance based on 2.91 and 3.36 Å found in the element (*13*) and most likely reflect only modest orbital overlap.

In order to simplify the conceptualization of the structure, the Sb(2)–Sb(2) and Zr–Zr geometric relationships have been emphasized at the expense of the stronger Sb–Zr bonds in the [100] projection of the structure shown in Fig. 1. The antimony(2) atoms form a puckered layer centered about {002} that is actually a slightly distorted version of the layers found for elemental antimony, albeit with greater interatomic distances (3.25 Å vs 2.91 Å). A clearer view of the layer is given in Fig. 2. Between these

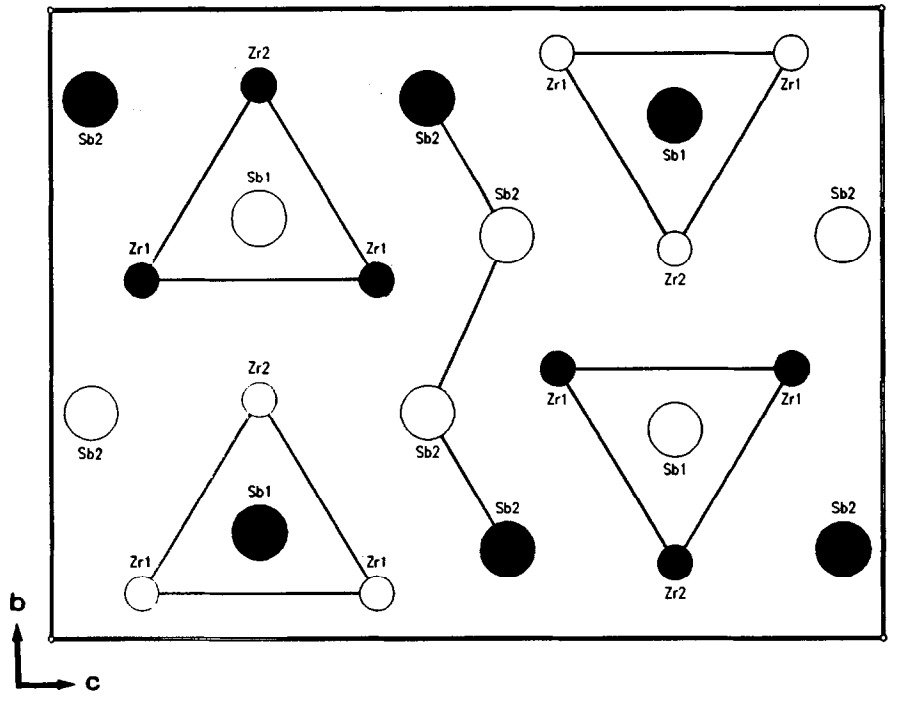

FIG. 1. Projection of the orthorhombic crystal structure of ZrSb along the short a-axis emphasizing Zr–Zr and Sb–Sb relationships. Shaded atoms are at $x = \frac{1}{2}$; open atoms are at $x = 0$. Many strong Zr–Sb contacts have been omitted in the interest of clarity.

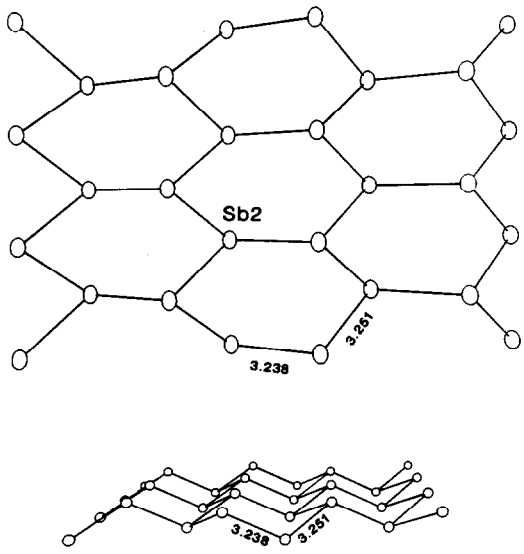

FIG. 2. Antimony(2) atoms in ZrSb form a layer that is distorted but very reminiscent of that found in elemental antimony (95% probability thermal ellipsoids).

layers lie columns composed of confacial trigonal prisms of zirconium atoms centered by antimony(1) atoms and with the pseudo-threefold axis parallel to [100]. Pairs of these columns displaced by $a/2$ are linked with 3.02 Å Zr(2)–Sb(1) contacts as well as by more numerous but weak Zr(1)–Zr(2) interactions at 3.40 Å. Comparable Zr–Zr separations of 3.39 Å also occur between columns separated by the antimony(2) layer. The resulting coordination involving only Zr–Sb bonding is shown in Fig. 3 for all of the atoms.

$ZrSb_{1.96}$. The β-phase has the $PbCl_2$ or anti-Co_2Si structure (*5*) that is already known to occur for ZrP_2 (*6*) and $ZrAs_2$ (*7*) from powder and single-crystal photographic work, respectively. Refined parameters are presented in Table IV. It should be noted that this phase appears to be substoichiometric in antimony, namely $ZrSb_{1.956(4)}$, as revealed by the nonunity value for the refined multiplicity of antimony(1). Such a property is also reminiscent of the pair of compounds at the equiatomic composition, viz. $ZrSb_{1-x}$ (FeSi) and ZrSb (ZrSb) (*1*). Unfortunately, the compositional dependence of the free energy of formation is not as well established in the present case since attempts to synthesize $ZrSb_{1.96}$ by sintering powders have produced only $ZrSb_2$ with the previously reported structure (*2*).

A projection of $ZrSb_{1.96}$ down the short b-axis is shown in Fig. 4 with the shorter Sb–Sb contacts emphasized. This structure allows close Sb(1)–Sb(1) contacts of 2.89 Å (Table IV) along an infinite zigzag chain parallel to the b-axis, with each atom in this chain also coordinated further to two antimony(2) atoms at 3.15 Å (Fig. 5). The antimony atoms also differ from above in their coordination to zirconium; antimony(1) is bonded to four zirconium atoms in a tetrahedral environment while antimony(2) is bonded to five zirconium atoms in a square pyramidal manner. The zirconium atom is

TABLE IV

REFINED PARAMETERS FOR AND DISTANCES IN $ZrSb_{1.956(4)}$ (β)

Atom	Site	Multipl.	x	y	z
Zr	4(c)	1.0	0.2606(1)	¼	0.1622(1)
Sb(1)	4(c)	0.956(4)	0.8713(1)	¼	0.04495(7)
Sb(2)	4(c)	1.0	0.9311(1)	¼	0.64586(7)

Interatomic distances (Å)[a]

Zr–1Sb(1)	2.923(1)	Sb(1)–2Sb(1)	2.890(1)
Zr–2Sb(1)	2.976(1)	Sb(1)–1Zr	2.923(1)
Zr–2Sb(2)	3.032(1)	Sb(1)–2Zr	2.976(1)
Zr–2Sb(2)	3.060(1)	Sb(1)–1Zr	3.091(1)
Zr–1Sb(1)	3.091(1)	Sb(1)–2Sb(2)	3.146(1)
Zr–1Sb(2)	3.209(1)	Sb(1)–1Sb(2)	3.731(1)
Zr–2Zr	3.987(1)	Sb(1)–1Sb(2)	3.849(1)
Sb(2)–2Zr	3.032(1)	Sb(1)–2Sb(2)	3.859(1)
Sb(2)–2Zr	3.060(1)	Sb(1)–2Sb(1)	3.987(1)
Sb(2)–2Sb(1)	3.146(1)		
Sb(2)–1Zr	3.209(1)		
Sb(2)–2Sb(2)	3.581(1)		
Sb(2)–1Sb(1)	3.731(1)		
Sb(2)–1Sb(1)	3.849(1)		
Sb(2)–2Sb(1)	3.859(1)		
Sb(2)–2Sb(2)	3.989(1)		

[a] Distances < 4.0 Å.

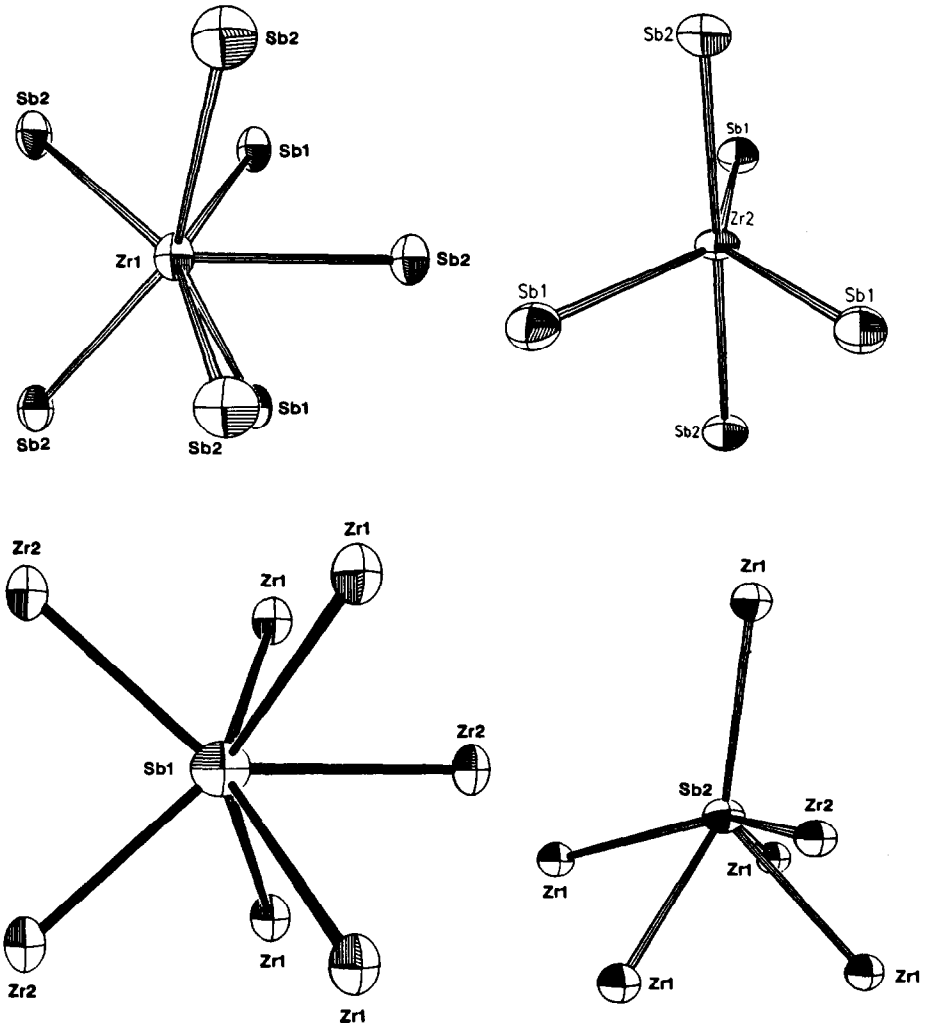

FIG. 3. Primary heteroatom coordination sphere of the four independent atoms in the ZrSb structure. Atom ellipsoids are drawn at the 95% probability level.

nine-coordinate, as would be expected in this structure, but one Zr–Sb(2) distance at 3.21 Å is significantly longer than the average of the other eight, 3.02 Å. The implications of some of these distances as well as the simplistic view of the structure as Zr^{4+} $Sb^{3-}Sb^{-}$ will be discussed below.

α-$ZrSb_2$. Comparable views of both the unit cell projection and ribbon of antimony atoms for the previously known $ZrSb_2$ structure (*2*) are shown in Figs. 6 and 7 (space group *Pnnm*, a = 14.9684(8) Å, b = 9.9672(6) Å, c = 3.8813(3) Å). It should be noted that the α-type structure contains twice as many formula units per unit cell as does the β ($PbCl_2$)-form. Here there are isolated pairs of Sb(4)–Sb(4) atoms in addition to short (2.88 Å) Sb(1)–Sb(1) separations within the antimony ribbon. The zirconium atoms are coordinated by eight antimony atoms in a bicapped trigonal prism in much the same manner as found for $ZrSb_{1.96}$ with

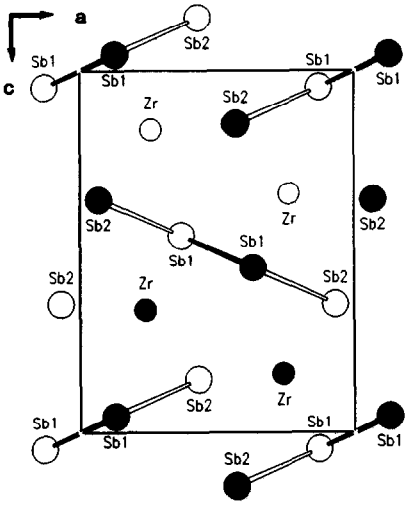

FIG. 4. Projection of the β-$ZrSb_2$ ($PbCl_2$-type) structure along the short b-axis. All atoms are at $y = \frac{1}{4}$ (open circles) or $y = \frac{3}{4}$ (filled circles). Antimony–antimony contacts have been emphasized.

the ninth atom now at a greater 3.4 Å. The coordination of the antimony atoms by zirconium and antimony near neighbors has also changed. With reference to Fig. 6, Sb(1) and Sb(2) have three zirconium neighbors, Sb(3) four, and Sb(4) six, compared with four and five atom coordination spheres observed in $ZrSb_{1.96}$. The increased Sb–Zr interaction by antimony(4) is compensated by a drop in Sb–Sb bonding so that it has only one antimony near neighbor (Fig. 6). The antimony atoms that are tetrahedrally bonded to four zirconium atoms are bonded to four Sb atoms in a square planar manner in both compounds (Sb(1) in $ZrSb_{1.96}$, Sb(3) in $ZrSb_2$). The remaining two antimony atoms in α-$ZrSb_2$ are both coordinated to three zirconium atoms but antimony(1) is bound to three antimony atoms while antimony(2) is bound to two.

The atomic numbering schemes used in the structural illustrations are also used in the presentation of the following calculational results.

Extended-Hückel Calculations

More meaningful comparisons of the two $ZrSb_2$ structures as well as a better definition of their bonding features and probable metallic characters can be obtained from the results of band calculations.

The density-of-states curve for $ZrSb_{1.96}$ is shown in Fig. 8 with the shaded areas under the curve representing the individual atom contributions of the three independent atoms in the structure to the total. Two broad bands appear below the Fermi energy (−8.7 eV). The lower one from −23 to −16 eV is mainly antimony s orbital in character with a very small zirconium contribution. The second band from −16 to −8.7 eV has a significant contribution from all three at-

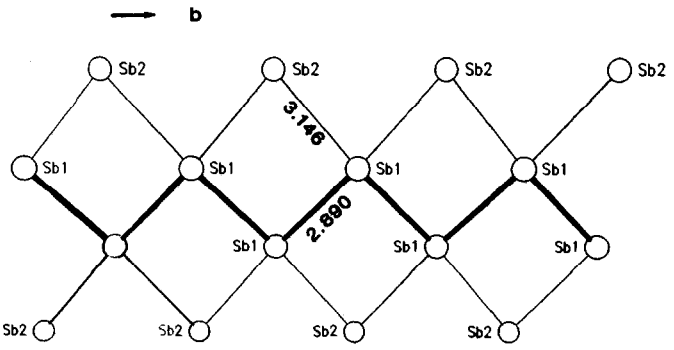

FIG. 5. The ribbon of antimony atoms in β-$ZrSb_2$.

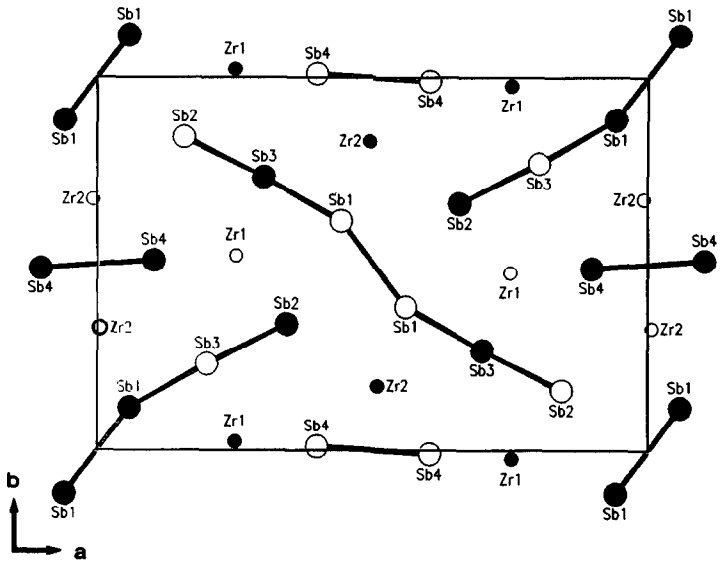

FIG. 6. Projection of the α-$ZrSb_2$ structure along the short c-axis. All atoms are at $z = 0$ (open circles) or $z = \frac{1}{2}$ (filled circles). Antimony–antimony contacts have been emphasized.

oms. The large degree of zirconium character in this band largely represents the extent of covalent interaction between antimony and zirconium since the Zr–Zr separations are all quite large. Located immediately above E_F is an empty band with a high DOS that is almost wholly zirconium in character. These three bands would be much narrower and have a great deal less mixing of the atomic states in any ionic description.

More insight into the bonding in β-$ZrSb_2$ can be obtained from Fig. 9 where the DOS curve has been overlap-weighted for various pairs of atoms such that a bonding interaction is positive and an antibonding one is negative. These crystal orbital overlap population (COOP) curves give a good representation of the bonding or antibonding effects for various atom pair interactions (*14*). Thus the Zr–Sb(1) and Zr–Sb(2) interactions can be seen to be strongly bonding up to the Fermi energy with the largest bonding component located in the upper valence band where there is significant zirconium mixing. It is also evident that there is not much to differentiate the two types of Zr–Sb interactions, and that the two antimony atoms interact in energetically nearly

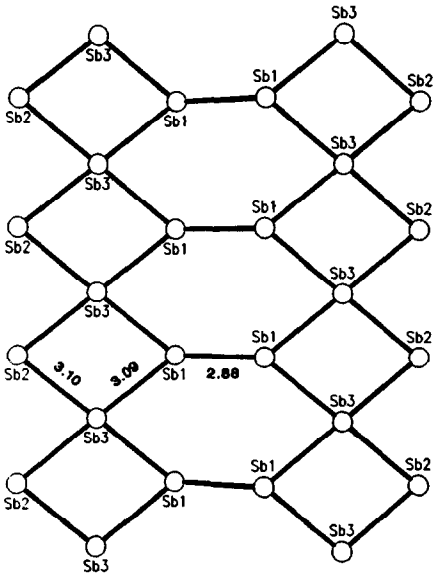

FIG. 7. The ribbon formed by three of four antimony atoms in α-$ZrSb_2$.

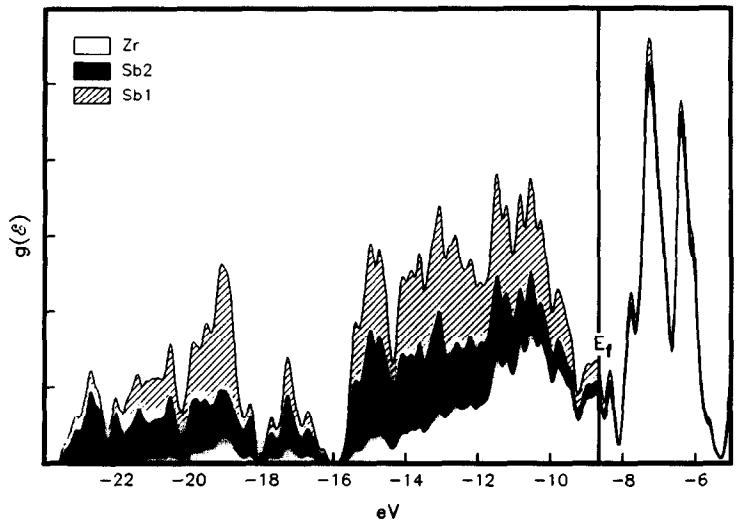

FIG. 8. DOS curve for β-$ZrSb_{1.96}$. The shaded areas under the curve represent the atomic orbital projections as indicated in the legend.

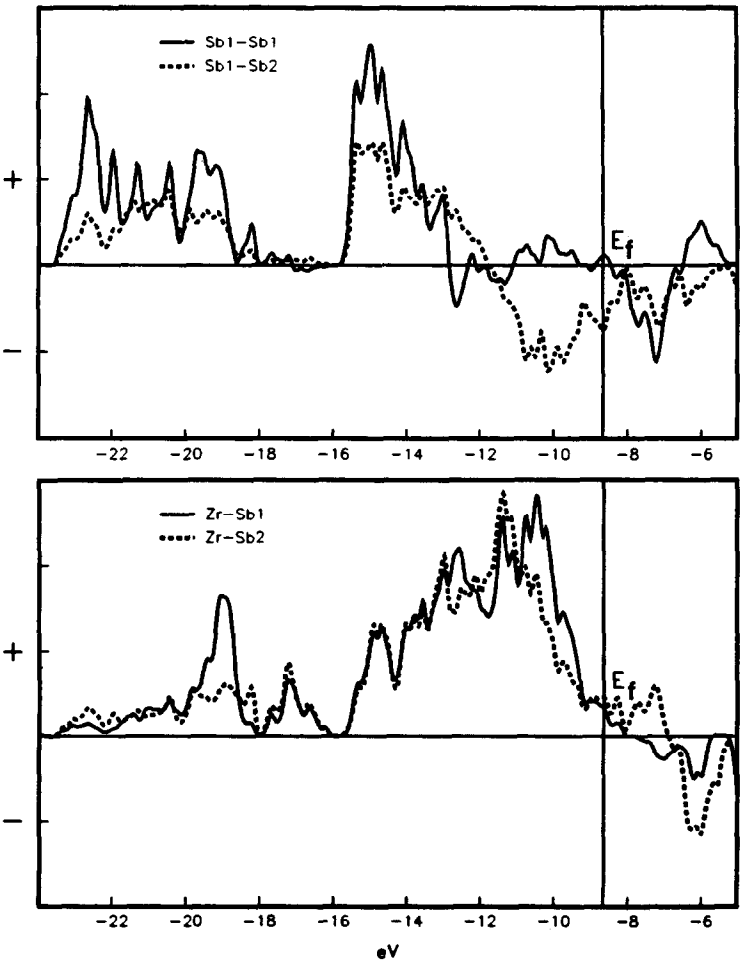

FIG. 9. COOP curves for β-$ZrSb_{1.96}$. The positive values on the curves represent bonding interactions while negative values denote an antibonding character for the atom pairs as indicated.

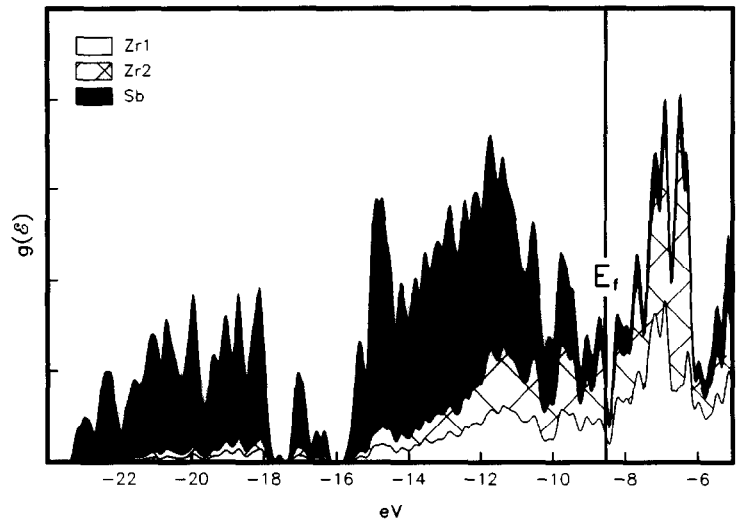

FIG. 10. DOS curve for α-$ZrSb_2$. The shaded areas under the curve represent the atomic orbital projections as indicated in the legend. In the interest of clarity all of the antimony projections have been summed and plotted as one.

equivalent ways with the metal atom. The COOP curves for the Sb–Sb interactions in Fig. 9 show that here there is a clear difference in the two atoms. The short Sb(1)–Sb(1) separation corresponds to strongly bonding components in both occupied bands of the DOS, but these are limited to the lower part of the higher (p) band, the remainder of the antimony orbitals being used for bonding to zirconium. The same can be said for Sb(1)–Sb(2) interactions in the energy region where Sb(1)–Sb(1) is bonding but now at a somewhat reduced level. However, above −13 eV there is a large antibonding component in the Sb(1)–Sb(2) COOP curve that is not seen for Sb(1)–Sb(1). This means weaker Sb(1)–Sb(2) interaction although a significant net positive overlap remains.

The results of the calculations for the other (α) $ZrSb_2$ modification are plotted in Figs. 10 and 11 in the same manner as above. In the interest of clarity and because the projections of the atomic contributions to the DOS curve are essentially the same for the antimony atoms, only the total is plotted in Fig. 10. Likewise, the sum of Zr(1)–Sb and Zr(2)–Sb interactions are plotted in Fig. 11. A comparison of the DOS curves for α-$ZrSb_2$ (Fig. 10) and $ZrSb_{1.96}$ (Fig. 8) shows that they are very similar. An antimony s-band between −23 and −16 eV, the antimony p-band admixed with a large amount of zirconium states between −16 and −8.5 eV, and the empty zirconium-dominated band just above the Fermi energy are all reproduced. The fact that the two compounds do not differ in major detail is not unexpected since subtle energy differences often determine which of a pair of structures is adopted.

The DOS curves for both structures would indicate that each should exhibit metal-like behavior. This is more certain in $ZrSb_{1.96}$ but since the Fermi level for α-$ZrSb_2$ falls just short of what appears to be a nonzero minimum, this finite DOS could be either an artifact of the Gaussian smoothing or the result of small errors in the calculations. In order to confirm a metallic behavior, the resistivity of $ZrSb_2$ was measured by a single-crystal four-probe technique

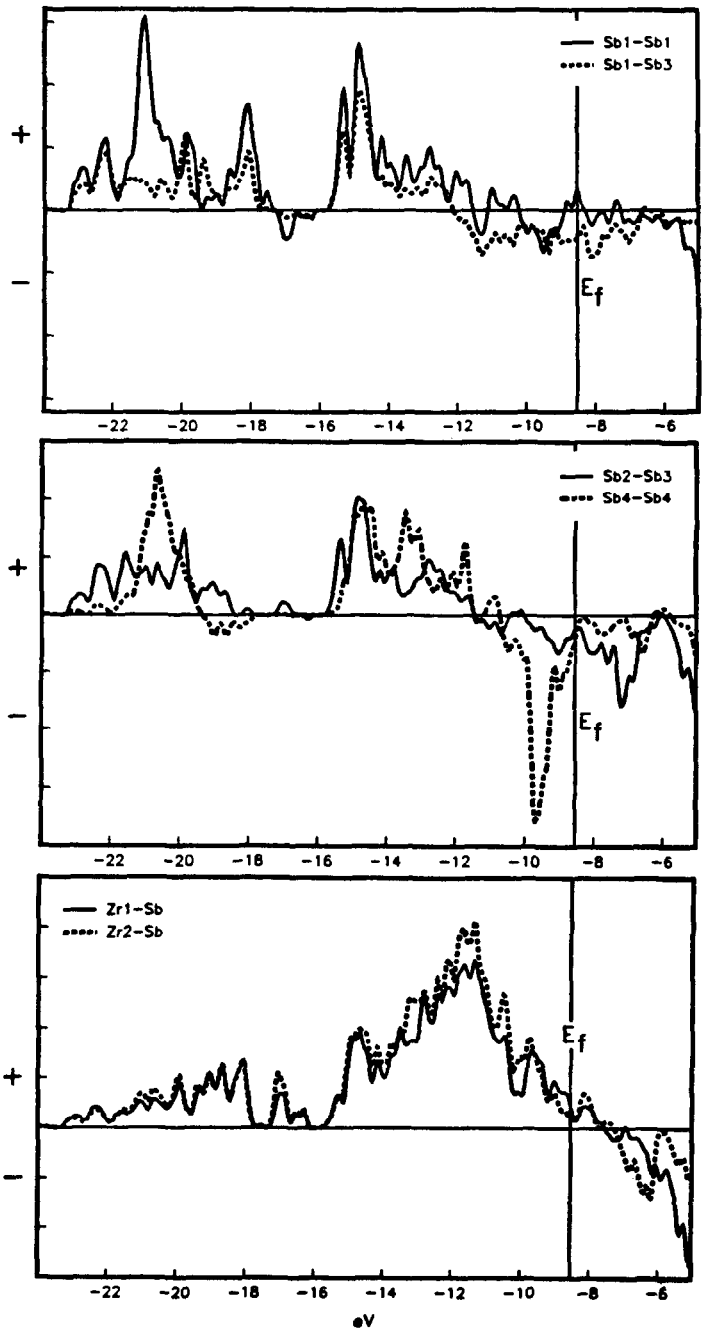

FIG. 11. COOP curves for α-$ZrSb_2$. The positive values on the curves represent bonding interactions while negative values denote an antibonding character for the atom pairs as indicated. Because the curves for Zr–Sb are very similar only the sum is plotted.

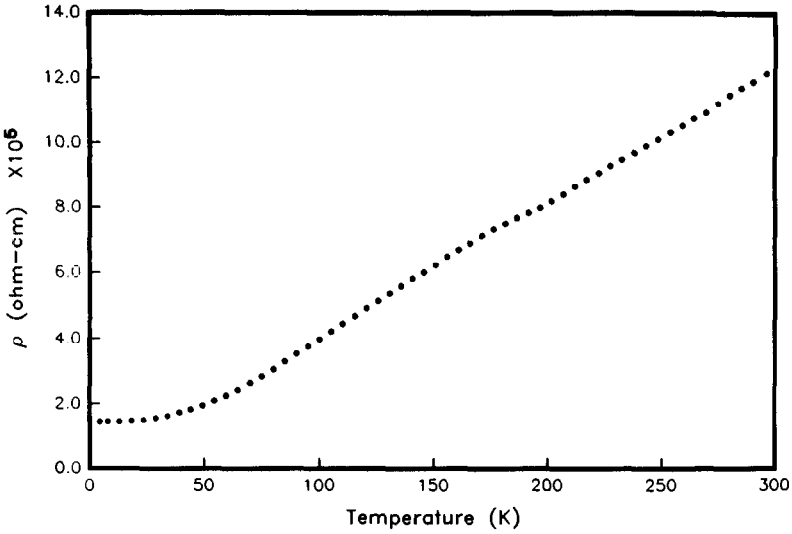

FIG. 12. Plot of the resistivity of α-$ZrSb_2$ along the antimony sheet (*c*) direction as a function of temperature.

along the antimony ribbon direction (*c*-axis, Fig. 6). The results are plotted in Fig. 12. The compound is indeed metallic, confirming a qualitative conclusion published by Hulliger (*15*). The room temperature resistivity of 1.2×10^{-4} ohm cm is an order of magnitude greater than that for the metal zirconium or the semimetal antimony.

Comparison of the COOP curves for the two diantimony compounds (Figs. 9 and 11) reveals that the Zr–Sb interactions are very similar, as suggested by the DOS curves. The observation is not as valid when comparing the interantimony interactions. There is a large narrow antibonding component 1 eV below E_F in the result for the α-$ZrSb_2$ structure, from the more distant Sb(4)–Sb(4) pair, that has no counterpart in the $PbCl_2$-type structure. In addition, the character of the other antimony interactions are weakly antibonding in the 2-eV region below the E_F for α-$ZrSb_2$ structure but only the Sb(1)–Sb(2) curve of the β-structure exhibits this behavior; the short and stronger Sb(1)–Sb(1) interaction in the latter is nonbonding in this region. The differences manifested in the Sb–Sb COOP curves are not surprising since the essential difference between the two structures involves Sb–Sb coordination.

Discussion

The numerous compounds in the zirconium–antimony system can be categorized as intermetallic, but this classification does not provide much insight into the electronic nature of the phases since many intermetallic compounds have strong ionic and covalent contributions to the bonding energy. The Zintl valence compounds (*16*) provide good examples of the latter. A good understanding of the zirconium–antimony compounds will require further study since the accompanying work (*1*) demonstrates that even such basic knowledge as the number and structure of the phases is not complete. Obviously, very little is known of the physical characteristics of these compounds. Some preliminary conclusions can be drawn from these synthetic and structural investigations, however.

Deducing the electronic nature of a compound solely from the crystal structure can be fraught with peril. The NaCl structure is found for such chemically diverse compounds as the alkali metal halides and transition metal carbides. This structure type is stable for different materials for different reasons. This is not always the case, however, since the diamond structure is found only for compounds with a strong covalent character to the interatomic bonding. In this manner, unique structure types found for Zr–Sb phases may provide insight beyond the "intermetallic" classification.

$ZrSb_2$ phases. The determination that a composition near $ZrSb_2$ can be found in the $PbCl_2$ structure is not in and of itself enlightening since $ZrSb_2$ and $PbCl_2$ are chemically sufficiently dissimilar to surmise that diverse factors determine the adoption of this structure. An examination of the resulting interatomic distances does provide further insight.

It is possible as a very crude approximation to describe β-$ZrSb_2$ as $Zr^{4+}Sb^{3-}Sb^{1-}$. In the very simple Zintl view, Sb^{3-} would have a complete octet of electrons and not form any covalent bonds to other antimony atoms, while Sb^{1-} would only need to be bonded to two other Sb atoms in order to satisfy the octet rule. This behavior for the nominal Sb^{1-} is observed in $CaSb_2$ where a zigzag chain analogous to that in elemental tellurium is formed (*17*). This chain is very similar to that formed by antimony(1) in $ZrSb_{1.96}$ [d(Sb–Sb) = 2.915 Å in $CaSb_2$ vs 2.890 Å in $ZrSb_2$] with the important difference that in the more reduced anion system each antimony(1) (chain) atom now is also a neighbor to two antimony(2) atoms at a longer but not insignificant 3.15 Å distance. (The 4% substoichiometry of the phase in antimony(1) also implies the chains are randomly segmented.) Since zirconium is less electropositive than calcium, the extent of electron transfer or ionicity should also be reduced, with a significant mixing of antimony p with zirconium d states. Neglecting the one long Zr–Sb contact at 3.21 Å, the bonding distances average at 3.02 Å, very typical of Zr–Sb interatomic separations in other binary compounds in this system. There are no significant Zr–Zr interactions, and so it can be stated that the lattice energy of $ZrSb_2$ in the $PbCl_2$ structure is derived mainly from Zr–Sb bonding but that a quite significant portion can be attributed to Sb–Sb bonding and that these main-group metal interactions are critical in the adoption of this structure.

The results of the extended-Hückel calculations for $ZrSb_{1.96}$ can be compared with the $Zr^{4+}Sb^{3-}Sb^{1-}$ formulation. The immediate breakdown of the ionic picture can be seen in the broad bands that exhibit significant amounts of Zr–Sb orbital mixing, and the band broadening produces overlap of the valence and conduction bands and, apparently, a metallic behavior. A more quantitative measure of the extent of charge transfer is obtained by integrating under the atomic projections in the DOS up to the Fermi level for each element. This gives a rough indication of the amount of electrons "owned" by each element, although the method characteristically often overestimates the polarity developed. These numbers listed in Table V for both $ZrSb_{1.96}$ and $ZrSb_2$ verify the limited polarity of these compounds.

The compounds also differ in their electrical properties from most Zintl phase compounds, which are semiconductors. This is not surprising since zirconium is much less electropositive than the alkali or alkaline earth metals often present in Zintl phases. [We note, however, that an important covalency for the heteroatomic bonds has also been estimated by theoretical means in compounds that contain lithium (*18–20*).] Despite the large difference in the magnitude of the assigned charges, $Zr^{4+}Sb^{3-}Sb^{1-}$ vs $Zr^{0.4+}Sb^{0.4-}Sb^{0}$, the antimony atom with fewer valence electrons compen-

TABLE V

ELECTRON TRANSFER AS ESTIMATED BY EXTENDED-HÜCKEL MEANS

	Atom	e/atom	Oxidation state
$ZrSb_{1.95}$	Zr	3.59	+0.41
	Sb(1)	4.77[a]	−0.02
	Sb(2)	5.39	−0.39
$ZrSb_2$	Zr(1)	3.59	+0.41
	Zr(2)	3.84	+0.16
	Sb(1)	5.05	−0.05
	Sb(2)	5.28	−0.28
	Sb(3)	4.76	+0.24
	Sb(4)	5.48	−0.48

[a] Sb(1) is substoichiometric and the calculations correspond to 95% occupancy (96% observed).

sates with more and stronger covalent interactions, especially within the antimony(1) chain (Fig. 5).

This formal charge reduction on the anions is doubtlessly important in the development of significant bonding among the different types of antimony atoms in both forms of $ZrSb_2$ (Figs. 5–7). This reflects a common tendency of the heavier elements in this part of the periodic table to formally expand their octets in electron-rich, multicenter bonding situations, giving in these cases a significant electron delocalization in the infinite antimony ribbons. The situation is reminiscent of the secondary interactions in elemental tellurium and many polyhalides and is more related to the bondings recently described for a variety of polytellurides (*21*). Though zirconium makes the major contribution to states at E_F in both forms of $ZrSb_2$, direct Zr–Zr interactions are also negligible, and significant contributions to conduction via bonding Zr–Sb as well as Sb(1)–Sb(1) interactions is implied by the COOP curves (Figs. 9 and 11).

When the structure goes from $PbCl_2$- to $ZrSb_2$-type, Zr–Sb interactions remain virtually identical as far as the zirconium is concerned since an appropriate coordination sphere of bicapped trigonal prisms can be found in both cases. However, since the connectivity of these trigonal prisms is different, the coordination of antimony by zirconium changes. The Sb–Sb interactions are also different in the two structures. When the β-type ($PbCl_2$) structure is compared with that of α-$ZrSb_2$, the average number of Zr–Sb bonds from each antimony changes from 4.5 to 4.0 with the average overlap population (integrated COOP curve) for each Zr–Sb bond increasing from 0.32 to 0.35 (Table VI). There are an average of three Sb–Sb interactions in the ribbon of antimony in both structures but the average overlap changes from 0.27 to 0.30. This increase of antimony bonding in the ribbon structure is compensated by the isolated Sb(4)–Sb(4) pair in the latter with an average overlap of only 0.18. In total, a small amount of Zr–Sb bonding is lost and a small amount of Sb–Sb bonding is gained when the structure type is changed from $PbCl_2$ to $ZrSb_2$ type.

With the exception of $TiAs_2$, the transition metal group IV diarsenides and diphosphides are found in the $PbCl_2$-type structure. Since the orbitals of phosphorus and arsenic have a smaller radial distribution compared with those for antimony and bismuth, the α-$ZrSb_2$ structure which sacrifices heteroatomic bonding in favor of homoatomic interactions would not be fa-

TABLE VI

AVERAGE PAIR-WISE OVERLAP POPULATIONS IN $ZrSb_2$ PHASES

β-$ZrSb_2$		α-$ZrSb_2$	
Sb(1)–Sb(1)	0.43	Sb(1)–Sb(1)	0.51
Sb(1)–Sb(2)	0.17	Sb(1)–Sb(3)	0.21
Zr–Sb(1)	0.30	Sb(2)–Sb(3)	0.29
Zr–Sb(2)	0.33	Sb(4)–Sb(4)	0.18
		Zr(1)–Sb(2)	0.37
		Zr(1)–Sb(1), Sb(3)	0.37
		Zr(1)–Sb(3), Sb(4)	0.26
		Zr(2)–Sb(1)	0.41
		Zr(2)–Sb(2), Sb(3)	0.33
		Zr(2)–Sb(4)	0.40

vored for the former. The exception occurs at $TiAs_2$ where the smaller sizes of both elements compensate. The larger and more metallic antimony and bismuth tend to favor the α-$ZrSb_2$ structure, and this is found for all zirconium and hafnium diantimonides and dibismuthides. The small size of titanium apparently renders both structures unstable; the compound $TiSb_2$ has the Al_2Cu structure (*5*), and no $TiBi_2$ phase has been found.

The observed interatomic distances and the calculations based thereon lead to the conclusion that the upper valence bands of both $ZrSb_2$ phases contain a considerable contribution from the antimony atoms. There is some charge transfer from the zirconium to antimony but to a much smaller extent than occurs in alkali or alkaline earth metal–antimony compounds. The Zintl phase concept is applicable only in the broadest sense in that the more covalently bonded antimony atoms carry a lesser amount of charge.

ZrSb. The exclusive ZrSb structure type may also occur for one more example, HfSb. Unreported powder pattern data for the compound have been indexed on the basis of an orthorhombic unit cell (a = 3.78, b = 10.36, c = 13.87 Å) (*22*) which is dimensionally quite similar to that of ZrSb.

In ZrSb there are no longer any short Sb–Sb distances, but the Zr–Zr distances are not significantly shorter either. It can therefore be surmised that Sb–Sb orbital overlap provides much less of a contribution to the stability of this compound and that Zr–Zr interactions are not significantly increased when compared to $ZrSb_2$. The greatest part of the lattice energy must be provided by Zr–Sb bonding. It seems likely that the states near the Fermi energy are weakly bonding Zr–Zr or Sb–Sb states. Despite the small contribution of these interactions to the total lattice energy they must play a critical role in the formation of this unique structure.

The second phase near the equiatomic composition is evidently substoichiometric and in the much more widely adopted FeSi structure type (*1*). This structural modification is not found exclusively for antimony compounds or even limited to those involving the phosphorus family. The majority of the 45 phases known to have this structure (*5*) are similar to FeSe, viz., compounds of 3*d* transition metals with Si, Ge, Sn, but compounds such as MgPt and AuBe also adopt this structure. This indicates that formation of the FeSi structure is not determined exclusively by electronic factors. It is interesting to note that even though this form is substoichiometric, $ZrSb_{1-x}$, it exhibits characteristics of a line compound. The very narrow ranges of lattice constants and compositional stability implies an inability of a structure to tolerate a varying electron count, which seems to contradict the previous assertion that the FeSi structure is not rigidly controlled by electronic factors. A noteworthy feature is the determinative effect of a small compositional variation on the formation of the FeSi or ZrSb structural modification. The dependence of these two as a function of other thermodynamic variables should yield interesting results, and these together with further physical characterization will provide a more quantitative insight than simple structural comparisons.

Zr_5Sb_3. The neighboring Zr_5Sb_{3+x} phase is remarkable not for the unique nature of its structure but rather for the widespread nature of its Mn_5Si_3-type structure. There are 294 phases, either binary or ternary, that have been reported to adopt it (*5*). This situation is analogous to the NaCl structure in which categorically contrasting interatomic interactions are accommodated by a single structure. The interstitial site probably plays a large role in the stability of the Mn_5Si_3 structure for many systems where a ternary (*Z*) atom may go undetected. The wide compositional stability range for

Zr_5Sb_{3+x} implies that the electronic states near the Fermi level are nonbonding and in a wide band and as such are able to tolerate a varying electron count. Such features are evident in the formation of a considerable variety of Zr_5Sb_3Z phases (*12*).

In contrast, a second Zr_5Sb_3 modification exhibits line compound behavior. This phase is found only in arc-melted samples and becomes metastable at low temperatures (<1100°C). Its Y_5Bi_3 structure type is not distinguished in Pearson from the Yb_5Sb_3 structure but the differences, albeit subtle, have been discussed (*23*). The number of compounds found with either of these structures is not large, 19, and they are so far exclusively adopted by compounds of the arsenic family with either the heavier rare-earth metals or the early transition metals. The structure type and small range of nonstoichiometry imply a strong electronic factor in the structure's stability.

An empty octahedral site reminiscent of that in the Mn_5Si_3 structure can also be found in Zr_2Sb. The analogy can be extended further since some compounds with the La_2Sb structure once thought to be binary phases were later shown to be impurity-stabilized ternary compounds, e.g., Ca_2Sb was determined to actually be Ca_4Sb_2O (*24*). However, the reproducible quantitative synthesis of Zr_2Sb indicates that such a stabilization is not required in the zirconium–antimony system. It seems certain that Zr–Zr interactions play the critical role in the formation of this structure that Sb–Sb interactions do in $ZrSb_2$. It also seems certain that the majority of the lattice energy again arises from Zr–Sb bonding. These same considerations also apply to the most zirconium-rich phase, Zr_3Sb.

Acknowledgments

The authors are indebted to R. A. Jacobson for the diffraction and computing facilities, P. Klavins and R. N. Shelton for assistance in resistivity measurements, and T. Hughbanks for help in running the extended-Hückel program.

References

1. E. Garcia and J. D. Corbett, *J. Solid State Chem.* **73,** 440 (1988).
2. A. Kjekshus, *Acta Chem. Scand.* **26,** 1633 (1972).
3. S.-J. Hwu, J. D. Corbett, and K. R. Poeppelmeier, *J. Solid State Chem.* **57,** 43 (1985).
4. P. Main, S. J. Fiske, S. E. Hull, L. Lessinger, G. Germain, J.-P. Declerg, and M. M. Woolfson, "MULTAN 80: A System of Computer Programs for the Automatic Solution of Crystal Structures from X-Ray Diffraction Data," Department of Physics, University of York, York (1980).
5. P. Villars and L. D. Calvert, "Pearson's Handbook of Crystallographic Data for Intermetallic Phases," Vol. 1–3, Amer. Soc. Met., Metal Park, OH (1985).
6. P. O. Snell, *Acta Chem. Scand.* **22,** 1942 (1968).
7. W. Trzebiatowski, S. Weglowski, and K. Lukaszewics, *Rocz. Chem.* **32,** 189 (1958).
8. R. Hoffmann, *J. Chem. Phys.* **39,** 1397 (1963).
9. T. Hughbanks and R. Hoffman, *J. Amer. Chem. Soc.* **105,** 1150 (1983).
10. G. Miller and J. Burdett, personal communication (1984).
11. H. Basch and H. B. Gray, *Theor. Chim. Acta* **4,** 367 (1966).
12. E. Garcia and J. D. Corbett, to be submitted for publication.
13. C. S. Barrett, P. Cucka, and K. Haefner, *Acta Crystallogr.* **16,** 451 (1963).
14. T. Hughbanks and R. Hoffman, *J. Amer. Chem. Soc.* **105,** 3531 (1983).
15. F. Hulliger, *Nature (London)* **204,** 991 (1964).
16. H. Schäfer and B. Eisenmann, *Rev. Inorg. Chem.* **3,** 29 (1981).
17. K. Deller and B. Eisenmann, *Z. Anorg. Allg. Chem.* **425,** 104 (1976).
18. A. Zunger, *Phys. Rev.* **17,** 2582 (1978).
19. T. Asada, F. Jarlborg, and A. J. Freeman, *Phys. Rev. B* **24,** 510 (1981).
20. M. C. Böhm, R. Ramirez, R. Nesper, and H.-G. v. Schnering, *Phys. Rev. B* **30,** 4870 (1984).
21. J. Bernstein and R. Hoffmann, *Inorg. Chem.* **24,** 4100 (1985).
22. W. Rossteutscher and K. Schubert, *Z. Metallkd.* **56,** 813 (1965).
23. Y. Wang, E. J. Gabe, L. D. Calvert, and J. B. Taylor, *Acta Crystallogr. Sect. B* **32,** 1440 (1976).
24. B. Eisenmann, H. Limartha, H. Schäfer, and H. A. Graf, *Z. Naturforsch. B* **35,** 1518 (1980).